Spiral holographic imaging through quantum interference

Jie Tang, Yang Ming, Wei Hu, and Yan-qing Lu

Citation: Appl. Phys. Lett. **111**, 011105 (2017); doi: 10.1063/1.4991365
View online: http://dx.doi.org/10.1063/1.4991365
View Table of Contents: http://aip.scitation.org/toc/apl/111/1
Published by the American Institute of Physics

Spiral holographic imaging through quantum interference

Jie Tang, Yang Ming,[a] Wei Hu, and Yan-qing Lu[a]
National Laboratory of Solid State Microstructures, College of Engineering and Applied Sciences, Collaborative Innovation Center of Advanced Microstructures, Nanjing University, Nanjing 210093, People's Republic of China

(Received 27 March 2017; accepted 20 June 2017; published online 5 July 2017)

Spiral holographic imaging in the Hong-Ou–Mandel interference scheme is introduced. Using spontaneous parametric down-conversion as a source of photon pairs, we analyze the joint orbital angular momentum spectrum of a reference photon and the photon encoding information of the object. The first-order interference of light beams in standard holographic imaging is replaced by the quantum interference of two-photon probability amplitudes. The difficulty in retrieving the amplitude and phase structure of an unknown photon is thereby avoided as classical interferometric techniques such as optical holography do not apply. Our results show that the full information of the object's transmission function can be recorded in the spiral hologram, which originates directly from the joint orbital angular momentum spectrum. This presents a lateral demonstration of compressive imaging and can potentially be used for remote sensing. *Published by AIP Publishing*. [http://dx.doi.org/10.1063/1.4991365]

The imaging of objects based on entangled photons was heuristically proposed by Belinskii and Klyshko[1] and developed in detail by Abouraddy.[2,3] Recently, the use of orbital angular momentum (OAM) states in this field has been extensively investigated. The high-dimensional OAM eigenstates have been exploited and found to be beneficial in many quantum information applications.[4,5] In imaging techniques, the use of OAM states has provided additional effects that enhance the sensitivity to particular features of an object. The two-dimensional spatial structure of the OAM mode basis enables imaging two-dimensional objects without needing pixel-by-pixel measurements, a method similar to compressive sensing.[6,7] In so-called digital spiral imaging,[8,9] the properties of an object are determined by analyzing the discrete OAM spectrum (or spiral spectrum) of the transmitted or reflected light. Ongoing research is exploring holographic ghost imaging with edge contrast enhancement,[10] the angular Fourier relationship between entangled photon pairs,[11,12] angular two-photon interference,[13,14] correlated spiral imaging,[15] and quantum digital spiral imaging.[16] Moreover, employing classical correlations of light instead of its quantum counterpart also allows the development of technologies with similar functionality to those utilize entangled photons.[17] It has been shown that using classical OAM correlations in random light, the spatial signatures and phase information of an object can be identified at any light levels.[18]

Note that these schemes are all based on ghost imaging techniques, where the reference and object arms are completely separated with recombination only required for coincidence counting. In contrast, for holographic imaging techniques, the object and reference arms are optically recombined prior to detection. In the classical scheme for holographic imaging, a coherent source is required to perform spatial interference between object and reference waves,[19] where a fixed phase relationship between the two beams is necessary.[20] Illuminating the object with entangled photon pairs precludes the application of these interferometric techniques. The entirely indeterminate global phase of a single photon makes it impossible to characterize the spatial structure of the photon that encodes the object information using conventional holographic imaging techniques.[21]

In this paper, we demonstrate a spiral hologram using photons that encode the full information of the transmission function of an object in the Hong-Ou–Mandel (HOM) interference scheme. The holographic imaging technique via first-order interference of light beams is replaced by the quantum interference of two-photon probability amplitudes by varying the distributions in the OAM representation. Any feature, such as the OAM spectrum, that distinguishes the photons will prevent the ideal two-photon coalescence from embodying the HOM effect. Therefore, the coincidence rate serves as a probe of the spatial structure of the photon that encodes the object information.

Before describing this spiral holographic imaging using HOM interference, we first recall the quantum scheme that corresponds to the quantum generalization of the plane-wave coherent field in classical holography. A two-photon entangled source is used, and a two-photon coincidence measurement is performed. The idler beam travels freely to one detector, and the signal beam reaches another after passing through the interferometer. In the interferometer, the signal field is divided into a reference and object wave.[22] The interference of the two two-photon wave-packets initiates the implementation of the quantum holographic scheme.

Consider now the HOM interference of OAM states. A set of OAM modes with different topological charges are represented as creation operators $a_m^\dagger$ and $b_n^\dagger$. The creation operator $a_m^\dagger$ acting on the vacuum state $|0\rangle$ creates a photon with OAM value m in path A (and A'); a similar interpretation holds for creation operator $b_n^\dagger$. The input state of a 50/50 beam splitter with one photon incident on each port

[a]Authors to whom correspondence should be addressed: njumingyang@gmail.com and yqlu@nju.edu.cn

can be decomposed into different transverse modes. The action of the 50/50 beam splitter for OAM modes induces a transformation

$$a_m^\dagger b_n^\dagger \rightarrow \frac{1}{2}\left(a_m^\dagger + b_m^\dagger\right)\left(b_n^\dagger - a_n^\dagger\right) = -\frac{1}{2}\left(a_m^\dagger a_n^\dagger + a_n^\dagger b_m^\dagger - a_m^\dagger b_n^\dagger - b_m^\dagger b_n^\dagger\right). \quad (1)$$

When measuring the OAMs l and l' of the photons that leave the two distinct output ports of the beam splitter simultaneously, we obtain the OAM-conditioned coincidence count rate $P(l_1, l_2)$. The coincidence events result from either reflection or transmission of both photons at the beam splitter (Fig. 1). These two indistinguishable events simultaneously contribute to the two-photon probability amplitude $\Psi(l_1, l_2)$, which describes one photon with OAM value l_1 and the other with OAM value l_2. It can be expressed as

$$\Psi(l_1, l_2) = \frac{1}{2}\left(\langle l_1|\psi_u\rangle\langle l_2|\psi_r\rangle - \langle l_2|\psi_u\rangle\langle l_1|\psi_r\rangle\right). \quad (2)$$

The joint probability distribution $|\Psi(l_1, l_2)|^2$ describes the non-destructive interference of the quantum paths of the reference photon and photon encoding the object information.

When identifying the object, similar to the linear momentum and linear position, the OAM and angular position form a pair of conjugate variables, related through the Fourier transform by[11]

$$A_l = \frac{1}{\sqrt{2\pi}}\int_{-\pi}^{\pi}\psi(\phi)\exp\left(-il\phi\right)d\phi,$$
$$\psi(\phi) = \frac{1}{\sqrt{2\pi}}\sum_{l=-\infty}^{\infty}A_l\exp\left(il\phi\right). \quad (3)$$

The state of the down-converted two-photon field is given by

$$|\psi\rangle = \sum_l C_l|l\rangle|-l\rangle. \quad (4)$$

$|l\rangle$ is an OAM eigenmode with helical phase $\exp(-il\phi)$ and C_l is the probability amplitude of finding a signal photon with OAM $l\hbar$ and an idler photon with $-l\hbar$. For the Gaussian mode pump condition, it produces the coefficients[15]

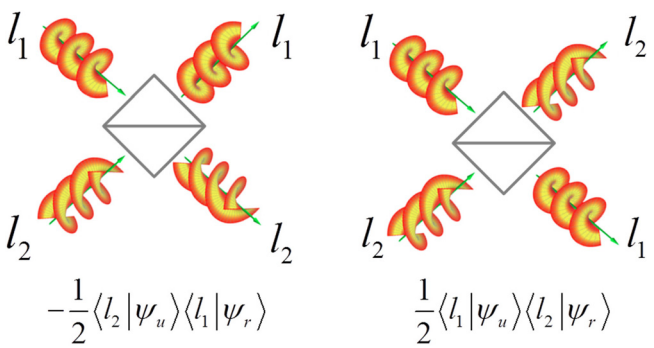

FIG. 1. Quantum interference of two photons in different OAM modes. The coincidence events (l_1, l_2) originate from the interference of the probability amplitudes produced under two scenarios. Here, we take $l_1 = 1, l_2 = 2$ as an example. Left: Both the reference photon with OAM value l_1 and the object-encoding photon with OAM value l_2 have been reflected from the beam splitter. Right: Transmission condition of two photons.

$$C_{p_1,p_2}^{l,-l} = \sum_{m=0}^{p_1}\sum_{n=0}^{p_2}\left(\frac{2}{3}\right)^{m+n+1}(-1)^{m+n} \times \frac{\sqrt{p_1!p_2!(l+p_1)(l+p_2)}(l+m+n)!}{(p_1-m)!(p_2-n)!(l+m)!(l+n)!m!n!}. \quad (5)$$

After the idler photon passes through the object, the two-photon state transforms as

$$|\psi'\rangle = \sum_l\sum_{k'}C_l A_{k',-l}|l\rangle|k'\rangle. \quad (6)$$

where the complex coefficient has the form[23]

$$A_{k,l} = \sqrt{\frac{2}{\pi|k|!}}\sqrt{\frac{2}{\pi|l|!}}\frac{1}{2} \times \int_0^\infty d\rho\int_0^{2\pi}d\phi\rho^{|k|+|l|+1}e^{-\rho^2}e^{-i\phi(k-l)}A(\rho,\phi). \quad (7)$$

As the idler photon is imparted with the phase of the object, the OAM spectrum is altered as well and represents the interaction of the correlated OAM state from spontaneous parametric down conversion (SPDC) with the object. These new OAM-mode distributions carry direct information of the object. To measure them, we can insert a beam splitter to mix the signal and idler photons. We then record the coincidence count rate of each detected OAM mode combination. As mentioned above, if the path information is erased, the specific combination detected arises from two possible conditions that interfere with each other. The input state from SPDC is transformed into

$$|\psi''\rangle = \sum_l\sum_{k'}\frac{1}{2}C_l A_{k',-l} \times \left(|l\rangle_a|k'\rangle_a - |l\rangle_b|k'\rangle_b + |k'\rangle_a|l\rangle_b - |l\rangle_a|k'\rangle_b\right). \quad (8)$$

The two-photon probability amplitude is then

$$\Psi(l_1, l_2) = {}_a\langle l_1|_b\langle l_2||\psi''\rangle = \frac{1}{2}\left(C_{l_2}A_{l_1,-l_2} - C_{l_1}A_{l_2,-l_1}\right), \quad (9)$$

with the corresponding joint probability distribution given by

$$\begin{aligned}P(l_1,l_2)\propto|\Psi(l_1,l_2)|^2 &= \frac{1}{4}\left|\left(C_{l_2}A_{l_1,-l_2} - C_{l_1}A_{l_2,-l_1}\right)\right|^2 \\ &= \frac{1}{4}C_{l_1}^2|A_{l_2,-l_1}|^2 + \frac{1}{4}C_{l_2}^2|A_{l_1,-l_2}|^2 \\ &\quad -\frac{1}{2}\mathrm{Re}\left(C_{l_1}C_{l_2}A_{l_1,-l_2}A_{l_2,-l_1}^*\right) \\ &= \frac{1}{4}C_{l_1}^2|A_{l_2,-l_1}|^2 + \frac{1}{4}C_{l_2}^2|A_{l_1,-l_2}|^2 \\ &\quad -\frac{1}{2}C_{l_1}C_{l_2}|A_{l_1,-l_2}A_{l_2,-l_1}^*|\cos(\phi_{12}-\phi_{21}),\end{aligned} \quad (10)$$

where we define

$$\phi_{12} = \arg(A_{l_1,-l_2}), \quad \phi_{21} = \arg(A_{l_2,-l_1}), \quad (11)$$

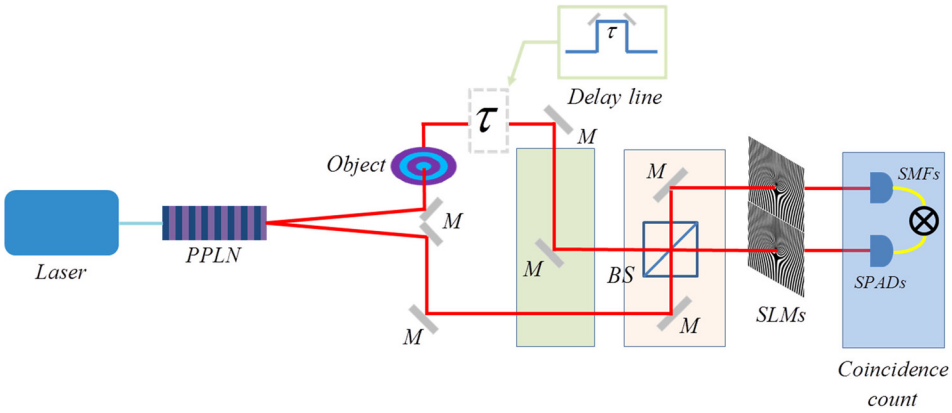

FIG. 2. Scheme of the proposed quantum spiral holographic imaging. A PPLN is illuminated by a 405-nm laser beam to generate OAM entangled photon pairs in a non-collinear manner. One of the photon pairs interacts with the object, and the other is set to be the reference. The photons are then passed through a 50/50 beam splitter from two distinct ports. An SLM together with a SMF in each arm is used to perform projective measurements of the OAM components.

as the phase of the complex coefficient for the corresponding OAM component. As the phase information is contained in the probability distribution, we actually have an instance of coherent imaging, similar to standard holography.

In the designed experimental setup (Fig. 2), a laser is used to pump periodically poled lithium niobate to down-convert the photon pairs entangled in their OAM degrees of freedom with type-I phase matching. The photons generated non-collinearly are easily separated, and they are prepared in the same spectral mode. The visibility of the HOM dip of photon pairs generated via the SPDC process characterizes the indistinguishability of their spectral (temporal) modes. It is determined by the properties of the entangled photon source, and here, we expect a visibility V= 100% for an ideal condition. However, in the practical situation, the HOM dip measurement often yields a visibility higher than 90% but always lower than 100%. The photons in path A are transmitted through the object to be imprinted on the local complex amplitude profile and the delay line to adjust the path length. Similar to the result mentioned in Ref. 24, the corresponding visibility depends on the transmission function of the object and is given by $V = \sum_{l=-\infty}^{\infty} P_l |A_{k,l}|^2$, where $A_{k,l}$ is defined as Eq. (7). The coefficient $|A_{k,l}|^2$ is always less than 1, yielding V less than the visibility of the HOM dip without an object. We set as a reference the photon in path B, where no transformation occurs before the beam splitter. The photons are then passed through a 50/50 beam splitter, followed by spatial light modulators encoded with phase-only holograms. When combined with single-mode optical fibers, these modulators enable projective measurements of particular OAM modes to be performed. The single-mode optical fibers are connected to avalanche photodiodes serving as single-photon detectors, and coincidences are registered using a coincidence counter. Note that we only measure the photons outgoing from the two distinct ports of the beam splitter.

As mentioned above, the spiral hologram of the object is obtained by recording $P(l_1, l_2)$. When recorded using conventional methods, the optical hologram is sensitive to the phase shift between the reference and the objective field. In contrast, when we record the hologram of the object using quantum interference, any constant offset of the local phase profile is entirely insensitive. If the transverse profile of the photon is expanded in the OAM eigenstates, this constant offset of the local phase profile does not alter the OAM spectrum of the photon. Therefore, the spiral hologram of the object we are recording here retains the same insensitivity as well.

We select the situation depicted in Fig. 3 to produce the simulation results of the spiral hologram of the object. We first investigate an object with an amplitude transmission function

$$A(\phi) = \begin{cases} 1, \text{ for } n\pi \le \phi \le \left(n\pi + \dfrac{\pi}{2}\right) \\ 0, \text{ else} \end{cases}. \tag{12}$$

We then choose the pure phase object with non-integer phase vortices. After scanning the OAM from $l = -7$ to $l = +7$, we obtain the simulation results presented in Fig. 4.

Let us consider the natural SPDC OAM joint probability distribution, meaning that the object is removed. Then, the state after the beam splitter is

$$|\psi\rangle = \frac{1}{2}\sum_l C_l\left(|l\rangle_a|-l\rangle_a - |l\rangle_b|-l\rangle_b + |-l\rangle_a|l\rangle_b - |l\rangle_a|-l\rangle_b\right). \tag{13}$$

Without the object, the strict correlations of the signal and idler photons forbid contributions of elements that violate OAM conservation. Hence, the probability distribution only features the diagonal term $\psi(l, -l) = \frac{1}{2}(C_{-l} - C_l)$. Moreover, it equals 0 because the coefficients obey the symmetry $C_l = C_{-l}$. Compared to the spiral hologram mentioned above, we find that an object can impart extra features in the probability distribution according to its azimuthal Fourier series.

We note in Eq. (5) that the commutation of l_1 and l_2 does not change the value of the joint probability, resulting in an

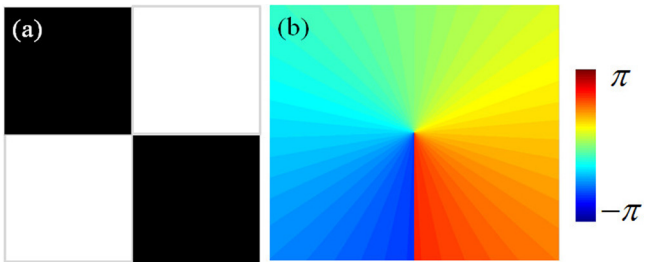

FIG. 3. Transmission profiles of the different objects. (a) The amplitude object with twofold rotational symmetries and its transmission function is described in Eq. (12); (b) the pure phase object consisting of a non-integer vortex with an winding number of M = −2/3.

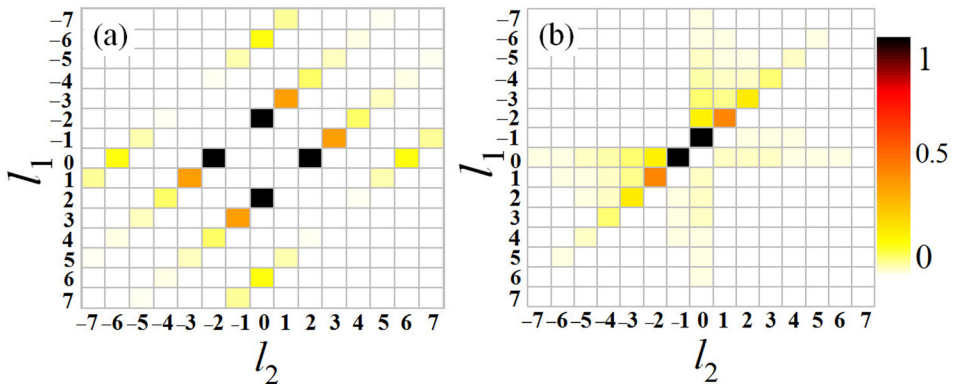

FIG. 4. Spiral hologram of the photon encoding the object information. The hologram reveals full information of the OAM spectral deviation with the initial SPDC states. (a) Depiction of the spiral hologram for photons passing the object with transmission profiles shown in Fig. 3(a). The largest coincidence count rate can be observed when $|l_1 - l_2| = 2$ due to the two-fold rotational symmetry of the object. (b) Spiral hologram for the pure phase object shown in Fig. 3(b). The presence of the phase object induces the OAM spectrum to be broader and changes the position of the joint probability central peak.

antisymmetric distribution along the diagonal line in the spiral hologram. The reason is that HOM interference permits only the antisymmetric component of the input state to produce coincidence counts in two distinct output ports.[25] At the exit facet of the nonlinear crystal, SPDC produces a symmetric OAM Bell state and naturally provides no contributions to the joint probability distribution. The object alters the OAM distribution of the incident photon, and the initial state is converted into a state with both symmetric and antisymmetric components. Objects with different transmission profiles convert the initial state in different ways, and their characteristic information, such as the OAM spectrum, receives antisymmetric components and is recorded in the joint probability distribution.

To reconstruct the object transmission function $A(\phi)$, we decode the expansion coefficients $A_{k,l}$ from the spiral hologram. The model of the complex coefficient $|A_{k,l}|$ can be obtained directly from the independent measurement. Moreover, following Eq. (5), we can use a numerical phase-retrieval method to find $\arg(A_{k,l})$ that most closely matches the spiral hologram (Fig. 4). This is equivalent to solving the optimization problem using the following procedure: $\min\|\,|\Psi(l_1,l_2)|^2 - |\Psi_{rec}^{(\arg(A_{k,l}))}(l_1,l_2)|^2\|$, where $\Psi_{rec}^{(\arg(A_{k,l}))}(l_1,l_2)$ is a functional defined by Eq. (5) and depends on the specific form of $\arg(A_{k,l})$.[26] Once the coefficients $A_{k,l}$ are found, image reconstruction can be implemented following the general idea suggested in other studies.

We now discuss the advantages and limitations of this holographic imaging technique. The HOM interference of spatial modes has been investigated previously.[27–29] One key point that has been analyzed is how the symmetry of the multimode pump beam affects the outcome of the HOM interference. The controlled engineering of two-photon high-dimensional entangled states has been demonstrated,[30] employing the HOM interference effect for the OAM basis, which is used here as precise OAM-state filters. Also, from the perspective of holographic imaging, the use of this particular effect is intended to record the spiral hologram of the encoding photon that is probed by the initial OAM correlated photon from SPDC. Furthermore, the difficulties associated with applying classical interferometric techniques are avoided. Instead of recording the spatial location information, detecting the OAM values requires much smaller numbers of measurements for specific objects, such as those with a rotationally symmetric phase profile. However, when scanning the limited range of OAM values (such as –7 to +7), we do not retrieve an identical transmission profile as the original object because of the unavoidable loss of spectral information. A more complete analysis needs to consider the radial field distribution, such as the p index in the LG basis, which requires further investigation. Low-photon flux of this scheme limits its applications in remote sensing. However, in the field where low light intensities are required, such as in biological imaging experiments with light-sensitive materials,[31] schemes based on quantum states of light can be feasible and useful. To protect the fragile quantum states of light, we can use the vortex fiber which is able to support multiple OAM modes with $l > 1$. Compared to propagation in the free space, it is an efficient compensating method to reduce the effect of noise and other de-coherence factors. The remarkable advantage of employing entangled photons is that correlations in the OAM degree of freedom are perfect. It provides a simple and direct way to analyze the spiral spectrum after various transformations. Entanglement enables the measurements to be done distantly, with the photons being spatially separated or even in unknown locations at some later time. By comparison, its classical counterpart which utilizes classical correlations in the angular position and OAM components of pseudothermal light shows many other advantages although these correlations are not perfect. It is possible to perform object identification at any light levels, an important advantage over the quantum protocols that employ fragile entangled states of light. What is more, their technique has shown that second-order interference effects are less sensitive to the coherence properties of the source.[17] Thus, the imaging schemes based on second-order correlations are robust against turbulence, a fundamental feature of any realistic scheme for remote sensing.

In conclusion, we have introduced a holographic method using HOM interference for quantum spiral imaging. The first-order interference of light beams is replaced by a spatial interference of two-photon probability amplitudes and then analyzed in the OAM representation. The spiral hologram of the encoded photon retains a sufficient amount of phase information of the complex coefficient of each OAM

component, enabling the full transmission function of the object to be retrieved. We focused on both the amplitude and the pure phase of the object, which can be easily generalized to objects with arbitrary complex transmission functions. This finding is expected to provide a promising platform for high-dimensional quantum holographic imaging and correlated OAM-based remote sensing.

This work was supported by the National Science Fund of China (Grant Nos. 61225026, 61322503, and 61490714), by the China Postdoctoral Science Foundation Funded Project (Grant No. 2016M590443), and by the Jiangsu Provincial Postdoctoral Foundation (Grant No. 1601170C).

[1]A. V. Belinskii and D. N. Klyshko, Sov. Phys. JETP **78**, 259 (1994), available at http://www.jetp.ac.ru/cgi-bin/e/index/e/78/3/p259?a=list.
[2]A. F. Abouraddy, B. E. A. Saleh, A. V. Sergienko, and M. C. Teich, Opt. Express **9**, 498 (2001).
[3]A. F. Abouraddy, P. R. Stone, A. V. Sergienko, B. E. A. Saleh, and M. C. Teich, Phys. Rev. Lett. **93**, 213903 (2004).
[4]N. V. Bloch, K. Shemer, A. Shapira, R. Shiloh, I. Juwiler, and A. Arie, Phys. Rev. Lett. **108**, 233902 (2012).
[5]Y. Ming, J. Tang, Z. X. Chen, F. Xu, L. J. Zhang, and Y. Q. Lu, IEEE J. Sel. Top. Quantum Electron. **21**, 6601206 (2015).
[6]E. J. Candes and M. B. Wakin, IEEE Signal Process. Mag. **25**, 21 (2008).
[7]O. Katz, Y. Bromberg, and Y. Silberberg, Appl. Phys. Lett. **95**, 13110 (2009).
[8]L. Torner, J. P. Torres, and S. Carrasco, Opt. Express **13**, 873 (2005).
[9]G. Molina-Terriza, L. Rebane, J. P. Torres, L. Torner, and S. Carrasco, J. Eur. Opt. Soc. **2**, 07014 (2007).
[10]B. Jack, J. Leach, J. Romero, S. Franke-Arnold, M. Ritsch-Marte, S. M. Barnett, and M. J. Padgett, Phys. Rev. Lett. **103**, 083602 (2009).
[11]B. Jack, M. J. Padgett, and S. Franke-Arnold, New J. Phys. **10**, 103013 (2008).
[12]A. K. Jha, B. Jack, E. Yao, J. Leach, R. W. Boyd, G. S. Buller, S. M. Barnett, S. Franke-Arnold, and M. J. Padgett, Phys. Rev. A **78**, 043810 (2008).
[13]A. K. Jha, J. Leach, B. Jack, S. Franke-Arnold, S. M. Barnett, R. W. Boyd, and M. J. Padgett, Phys. Rev. Lett. **104**, 010501 (2010).
[14]L. X. Chen, J. Leach, B. Jack, M. J. Padgett, S. Franke-Arnold, and W. L. She, Phys. Rev. A **82**, 033822 (2010).
[15]D. S. Simon and A. V. Sergienko, Phys. Rev. A **85**, 043825 (2012).
[16]L. X. Chen, J. Lei, and J. Romero, Light: Sci. Appl. **3**, e153 (2014).
[17]O. S. Magana-Loaiza, M. Mirhosseini, R. M. Cross, S. M. H. Rafsanjani, and R. W. Boyd, Sci. Adv. **2**, e1501143 (2016).
[18]Z. Yang, O. S. Magana-Loaiza, M. Mirhosseini, Y. Y. Zhou, B. S. Gao, L. Gao, S. M. H. Rafsanjani, G. L. Long, and R. W. Boyd, "Digital spiral object identification using random light," Light: Sci. Appl. (to be published).
[19]D. Gabor, Nature **161**, 777 (1948).
[20]T. Kobayashi, R. Ikuta, S. Yasui, S. Miki, T. Yamashita, H. Terai, T. Yamamoto, M. Koashi, and N. Imoto, Nat. Photonics **10**, 441 (2016).
[21]A. I. Lvovsky, H. Hansen, T. Aichele, O. Benson, J. Mlynek, and S. Schiller, Phys. Rev. Lett. **87**, 050402 (2001).
[22]X. B. Song, D. Q. Xu, H. B. Wang, J. Xiong, X. Zhang, D. Z. Cao, and K. Wang, Appl. Phys. Lett. **103**, 131111 (2013).
[23]N. Uribe-Patarroyo, A. Fraine, D. S. Simon, O. Minaeva, and A. V. Sergienko, Phys. Rev. Lett. **110**, 043601 (2013).
[24]H. Di Lorenzo Pires, H. C. B. Florijn, and M. P. van Exter, Phys. Rev. Lett. **104**, 020505 (2010).
[25]S. P. Walborn, A. N. de Oliveira, S. Pádua, and C. H. Monken, Phys. Rev. Lett. **90**, 143601 (2003).
[26]M. Servin, J. L. Marroquin, and F. J. Cuevas, Appl. Opt. **36**, 4540 (1997).
[27]E. Nagali, F. Sciarrino, F. de Martini, L. Marrucci, B. Piccirillo, E. Karimi, and E. Santamato, Phys. Rev. Lett. **103**, 013601 (2009).
[28]M. Jachura and R. Chrapkiewicz, Opt. Lett. **40**, 1540 (2015).
[29]E. Karimi, D. Giovannini, E. Bolduc, N. Bent, F. M. Miatto, M. J. Padgett, and R. W. Boyd, Phys. Rev. A **89**, 013829 (2014).
[30]Y. Zhang, F. S. Roux, T. Konrad, M. Agnew, J. Leach, and A. Forbes, Sci. Adv. **2**, e1501165 (2016).
[31]R. Fickler, R. Lapkiewicz, W. N. Plick, M. Krenn, C. Schaeff, S. Ramelow, and A. Zeilinger, Science **338**, 640 (2012).